Ying Liu,[1] Rengasamy Palanivel,[1] Esther Rai,[1] Min Park,[1] Tim V. Gabor,[1] Michael P. Scheid,[1] Aimin Xu,[2] and Gary Sweeney[1]

Adiponectin Stimulates Autophagy and Reduces Oxidative Stress to Enhance Insulin Sensitivity During High-Fat Diet Feeding in Mice

Diabetes 2015;64:36–48 | DOI: 10.2337/db14-0267

Numerous studies have characterized the antidiabetic effects of adiponectin, yet the precise cellular mechanisms in skeletal muscle, in particular, changes in autophagy, require further clarification. In the current study, we used a high-fat diet (HFD) to induce obesity and insulin resistance in wild-type (WT) or adiponectin knockout (Ad-KO) mice with and without adiponectin replenishment. Temporal analysis of glucose tolerance and insulin sensitivity using hyperinsulinemic-euglycemic clamp and muscle insulin receptor substrate and Akt phosphorylation demonstrated exaggerated and more rapid HFD-induced insulin resistance in skeletal muscle of Ad-KO mice. Superoxide dismutase activity, the reduced glutathione-to-glutathione disulfide ratio, and lipid peroxidation indicated that HFD-induced oxidative stress was corrected by adiponectin. Gene array analysis implicated several antioxidant enzymes, including Gpxs, Prdx, Sod, and Nox4, in mediating this effect. Adiponectin also attenuated palmitate-induced reactive oxygen species production in cultured myotubes and improved insulin-stimulated glucose uptake in primary muscle cells. Increased LC3-II and decreased p62 expression suggested that HFD induced autophagy in muscle of WT mice; however, these changes were not observed in Ad-KO mice. Replenishing adiponectin in Ad-KO mice increased LC3-II and Beclin1 and decreased p62 protein levels, induced fibroblast growth factor-21 expression, and corrected HFD-induced decreases in LC3, Beclin1, and ULK1 gene expression. In vitro studies examining changes in phospho-ULK1 (Ser555), LC3-II, and lysosomal enzyme activity confirmed that adiponectin directly induced autophagic flux in cultured muscle cells in an AMPK-dependent manner. We overexpressed an inactive mutant of Atg5 to create an autophagy-deficient cell model, and together with pharmacological inhibition of autophagy, demonstrated reduced insulin sensitivity under these conditions. In summary, adiponectin stimulated skeletal muscle autophagy and antioxidant potential to reduce insulin resistance caused by HFD.

Adiponectin normally circulates abundantly in the concentration range of 2 to 20 μg/mL, and decreased plasma adiponectin, in particular the high-molecular-weight form, has been found in patients with obesity and type 2 diabetes (1). Extensive studies have shown that adiponectin exerts beneficial antidiabetic actions by direct metabolic and insulin-sensitizing effects in various tissues (2). Skeletal muscle is the major site for glucose disposal, and maintenance of insulin sensitivity is critical for optimal glucose homeostasis. Generation of reactive oxygen species (ROS) and the resulting oxidative stress, mitochondrial dysfunction, and accumulation of triglyceride and lipotoxic metabolites have all been shown to contribute to insulin resistance (3,4). Transgenic mice overexpressing adiponectin show improved insulin sensitivity and mitochondrial function (5,6), whereas adiponectin knockout (Ad-KO) mice are more susceptible to insulin resistance induced by a high-fat diet (HFD).

[1]Department of Biology, York University, Toronto, ON, Canada
[2]State Key Laboratory of Pharmaceutical Biotechnology and Department of Medicine, the University of Hong Kong, Hong Kong
Corresponding author: Gary Sweeney, gsweeney@yorku.ca.

Received 17 February 2014 and accepted 24 July 2014.
This article contains Supplementary Data online at http://diabetes.diabetesjournals.org/lookup/suppl/doi:10.2337/db14-0267/-/DC1.

In response to cellular stressors, increased levels of autophagy permit cells to efficiently adapt by altering protein catabolism; however, autophagy is viewed as a double-edged sword, with too much or too little, and the temporal nature of the process determining cellular consequences (7,8). Several studies have recently begun to establish the importance of autophagy in skeletal muscle metabolism. In autophagy-deficient mice with skeletal muscle–specific deletion of Atg7, the induction of Fgf21 expression in muscle mediated peripheral effects, leading to protection from diet-induced obesity and insulin resistance (9). Another mouse model of stimulus-deficient autophagy, the BCL2 AAA mice, which contain knock-in mutations in BCL2 phosphorylation sites (Thr69Ala, Ser70Ala, and Ser84Ala) that prevent autophagy activation, showed altered glucose metabolism during acute exercise and impaired chronic exercise–mediated protection against HFD-induced glucose intolerance (10). Others have reported activation of autophagy in skeletal muscle in response to exercise and caloric restriction (11–14). The ability to induce autophagy has been shown to deteriorate with aging in skeletal muscle (15). Thus, recent literature suggests that induction of skeletal muscle autophagy by various stimuli may give rise to beneficial metabolic effects. Numerous studies have also established the importance of crosstalk between autophagy and oxidative stress (16).

That adiponectin exerts beneficial metabolic effects by direct actions and enhancing insulin sensitivity (2) is clear; however, the underlying molecular mechanisms are incompletely understood. We used Ad-KO mice fed an HFD for 2, 4, and 6 weeks, with and without adiponectin replenishment, to examine the corrective effects of adiponectin in this model. We examined changes in oxidative stress and underlying mechanisms and also established that adiponectin directly stimulates autophagy in skeletal muscle. These studies provide new insight into skeletal muscle actions of adiponectin that contribute to the beneficial antidiabetic effects of this adipokine.

RESEARCH DESIGN AND METHODS

Reagents and Antibodies

^{3}H-2-deoxy-glucose was purchased from PerkinElmer (Woodbridge, ON, Canada). Insulin (Humulin R) was purchased from Eli Lilly and Company (Toronto, ON, Canada). TRIzol reagent was from Invitrogen Life Technologies (Burlington, ON, Canada). Polyclonal phosphospecific antibodies to Akt (Thr308, Ser473) and ULK1 (Ser555), LC3B, Beclin1, GAPDH, and horseradish peroxidase–conjugated anti–rabbit-IgG were from Cell Signaling Technology (Beverly, MA). Polyclonal phosphospecific antibody to IRS1 (Y612) was from Life Technologies, p62 antibody was from BD Biosciences (Mississauga, ON, Canada), and fibroblast growth factor (FGF)-21 antibody was from Antibody Immunoassay Services (Hong Kong). Polyvinylidene difluoride membrane was from Bio-Rad Laboratories, Inc. (Burlington, ON, Canada), and chemiluminescence reagent plus was from PerkinElmer (Boston, MA). Alpha-minimal essential medium and FBS were purchased from GIBCO, Invitrogen Life Technologies (Burlington, ON, Canada). All other reagents and chemicals used were of the highest purity available.

Experimental Animals, Glucose Tolerance Tests, and Hyperinsulinemic-Euglycemic Clamp

Animal facilities met the Canadian Council on Animal Care Guidelines, and the York University Animal Care Committee approved the protocols. Animals were fed a regular chow diet or 60% HFD as we described (17). HFD Ad-KO animals received saline or adiponectin (3 μg/g body weight) twice daily for 1 and 2 weeks for the 2-week and 6-week diet groups, respectively, by intraperitoneal injection. Glucose tolerance tests (GTT) and clamp studies were performed as we described (17).

Preparation of Muscle Homogenates, Cell Lysates, and Western Blotting

Stably transfected L6 cells were serum-starved 4 h and incubated with or without bafilomycin (200 nmol/L, 24 h), chloroquine (100 μmol/L, 24 h), and compound C (10 μmol/L, 1 h), followed by insulin stimulation (10, 100 nmol/L, 5 min) or adiponectin (5 μg/mL, 30 and 60 min) treatment. All tissue and cell samples were prepared as we described before (17), and primary antibodies were used at 1:1,000 dilutions. Membranes were washed four times in 1× wash buffer for 15 min each at room temperature and incubated with appropriate horseradish peroxidase-coupled secondary antibody (1:10,000) for 1 h. Membranes were washed five times in 1× wash buffer for 10 min each and proteins visualized using enhanced chemiluminescence. Nondenaturing, nonreducing conditions were applied to allow analysis of different forms of adiponectin (high molecular weight >250 kDa, medium molecular weight = 180 kDa, and low molecular weight = 90 kDa) with in-house polyclonal anti-adiponectin antibody in the concentration of 1 μg/mL and anti-rabbit as the secondary antibody. Quantitation of each specific protein band was determined by densitometric scanning and correction for the respective loading control.

Superoxide Dismutase Activity Assay

Tissue-specific superoxide dismutase (SOD) activity was assessed with the colorimetric Superoxide Dismutase Activity Assay Kit purchased from BioVision, Inc. (Milpitas, CA). Gastrocnemius skeletal muscle samples were crushed into powder in liquid N_2, and protein was extracted according to the manufacturer's instructions. Approximately 10 μg protein from each sample was used to measure SOD activity under optical density of 450 nm by a microplate photometric reader. Data represented in the RESULTS were normalized for protein concentration loaded for each sample.

Glutathione Assay

Tissue-specific total and reduced glutathione (GSH) levels were analyzed with the ApoGSH Glutathione Colorimetric

Detection Kit from BioVision. Tibialis anterior (TA) skeletal muscle samples were crushed into powder in liquid N_2, and protein was extracted according to the manufacturer's instructions. The same volume of lysate for each sample was used to determine total and reduced GSH level, and a microplate photometric reader was used to read the assay at 412 nm. Data represented in the RESULTS were normalized by protein concentration loaded for each sample.

Thiobarbituric Acid Reactive Substances Assay

Tissue-specific lipid peroxidation level was analyzed with a thiobarbituric acid reactive substances (TBARS) assay kit from Cayman Chemical Co. (Ann Arbor, MI). TA skeletal muscle samples were crushed into powder in liquid N_2, and protein was extracted according to the manufacturer's instructions. In total, 600 μg protein from each tissue sample lysate was used to determine TBARS and the assay read at 540 nm by a microplate photometric reader. Data represented in RESULTS were normalized by protein concentration loaded for each sample.

Oxidative Stress–Related and Autophagy-Related Gene Expression Analysis

Gastrocnemius skeletal muscle samples collected from animals were crushed to powder in liquid N_2, and total RNA was extracted with TRIzol reagent (Invitrogen Life Technologies) and cleaned up by RNEasy Mini Kit (Qiagen, Toronto, ON, Canada). cDNAs were synthesized by reverse transcription with 1 μg total RNA by using the RT^2 First-Stand cDNA Synthesis Kit (Qiagen). A mixture of cDNAs and RT^2 qPCR Master Mix was aliquoted to 96-well plates precoated with primers encoding different genes involved in the regulation of the oxidative stress pathway (Qiagen). The plate was loaded onto a quantitative PCR machine, and the real-time PCR program was set according to the company's instructions. Results were collected from each well after quantitative PCR was adjusted by several housekeeping genes, including GAPDH and β-actin, before being analyzed.

For analysis of autophagy-related gene expression, RNA (0.2 μg) was reverse-transcribed in a 20-μL reaction volume using specific primers (Invitrogen) listed in Supplementary Table 1 and GoScript reverse transcriptase according to the manufacturer's instructions (Promega). RT-PCR was performed with KAPA Polymerase Chain Reaction Master Mix (Kapa Biosystems Inc., Wilmington, MA) and SYTO 9 Green Fluorescent Nucleic Acid Stain (Life Technologies) under standard thermocycling conditions (2 min at 95°C, followed by 40 cycles of 5 s each at 95°, 60°, and 72°C). Relative expression levels of genes, normalized using β-actin as a housekeeping gene, were calculated using the comparative critical threshold method.

Immunofluorescent Analysis of Endogenous LC3

Analysis of LC3 cellular localization was performed by culturing cells on glass cover slips and treating with adiponectin for 1 and 2 h. Thereafter, the media were aspirated and the cells were washed (three times) in PBS at room temperature and then fixed for 20 min in 4% paraformaldehyde at room temperature, then further washed (three times for 5 min) with PBS. Cells were permeabilized with 0.1% Triton X-100 for 3 min and blocked with blocking buffer (3% BSA) for 30 min. After fixation, permeabilization, and blocking, the cells were washed once in PBS and then sequentially stained with LC3 primary antibody (1:1000) overnight at 4°C and then secondary-antibody conjugated with Alexa Fluor 488 (1 h at room temperature). Cells were then washed with PBS before incubation with 2 μg/mL DAPI (Roche Diagnostics) in PBS for 20 min at room temperature. The samples were washed with PBS (four times) and mounted with Dako fluorescence mounting medium (Dako North America Inc., Carpinteria, CA) and observed with an Olympus confocal microscope equipped with a ×60 objective.

Cell Culture Using L6 and Primary Skeletal Muscle Cells

We used the L6 skeletal muscle cell line grown as previously described (18) for some in vitro studies as indicated in the figure legends. To prepare primary skeletal muscle cells, we also isolated muscle strips from mouse hind leg and cut them into small pieces, which were then incubated in 3 mL dispase/collagenous solution (0.1 type II collagenase + 0.05% dipase in serum-free Ham's F12 media) for 30 min in a 37°C water bath with agitation (~100 rpm). Digested solutions were filtered through a 100-μm cell filter, and only flow through was collected and centrifuged at room temperature for 7 min at 1,600 rpm. The cell pellet was resuspended in growth media (10% FBS, 0.5% antibiotics and antimycotics, 5 ng/mL recombinant human FGF in Ham's F12) and plated onto a 35-mm dish overnight. The nonadherent cells in the supernatant were then seeded on a laminin-coated 35-mm dish. These cells were differentiated into myotubes in Ham's F12 media containing 2% horse serum for 5–7 days, and experiments were performed using fully differentiated myotubes.

Generation of L6 Cell Line With Stable Overexpression of Tandem Red Fluorescent Protein/Green Fluorescent Protein–LC3 (tfLC3) or ATG5-K130R by Retroviral Infection

We used the L6 skeletal muscle cell line for in vitro studies. After identifying relevant and unique restriction sites matching with the retroviral cloning vector pQCXIP and the red fluorescent protein (RFP)/green fluorescent protein (GFP)–LC3 target vector, ptfLC3 (Addgene), we successfully generated and purified the retroviral vector expressing the gene of interest, tfLC3, and all other essential elements for retroviral integration and expression. We also subcloned the target RFP-ATG5-K130R sequence from the vector pmCherry-ATG5-K130R (Addgene) into the vector pQCXIP. In both cases, the viral vector was then transfected into the human embryonic kidney–derived packaging cell line, EcoPack 2-293 (Clontech Laboratories, Inc.), expressing the Moloney murine leukemia virus Gag, Pol, and Env proteins. The culture medium containing the

virus was collected 48 h after transfection, and 100 μL of the collected supernatant, or viral soup, was directly applied to L6 cells in the presence of polybrene (4 μg/mL) in a 10-cm culture dish the next day after being seeded. Cells were incubated with the virus for 24 h in the incubator, and the medium was replaced with fresh growth medium containing the selection antibiotic, puromycin (2 μg/mL; Sigma-Aldrich). The pool of cells resistant to the antibiotic was selected, and the stable overexpression of the target gene was verified by detecting the expression of GFP using FACSCalibur flow cytometry (BD Bioscience).

Analysis of Autophagic Flux Using Tandem RFP/GFP-LC3

L6 cells stably transfected with tfLC3 were seeded on glass cover slips. Cells were maintained in culture medium until reaching 70–80% confluence and then treated with adiponectin (5 μg/mL up to 24 h). Cells were washed with PBS and fixed with 4% paraformaldehyde for 20 min, followed by permeabilization with 0.1% Triton X-100 for 3 min. Cells were blocked with PBS containing 3% BSA for 30 min at room temperature. Coverslips were washed three times with PBS and mounted with Dako fluorescence mounting medium (Dako North America Inc.), and GFP and RFP fluorescence was detected by confocal microscopy.

Analysis of Cathepsin B Activity Using Magic Red

L6 cells were cultured on glass coverslips and treated with adiponectin for 1 h and 2 h; then, lysosomal activity was determined with the Magic Red Cathepsin B kit (ImmunoChemistry Technologies, Bloomington, MN) according to the manufacturer's instructions. Nuclei were counterstained with DAPI for 20 min. After being washed four times with PBS, cells were mounted with Dako fluorescence mounting medium, and images were observed with an Olympus confocal microscope equipped with a ×60 objective.

2-Deoxy-Glucose Uptake

L6 myoblasts stably overexpressing GLUT4-myc (18) were incubated with media containing 0.5% FBS, with or without bafilomycin (200 nmol/L, 24 h) or chloroquine (100 μmol/L, 24 h), followed by insulin (10 and 100 nmol/L, 20 min). After treatments, glucose uptake was determined as previously described (18).

Statistical Analysis

All data were analyzed by using GraphPad Prism 5 software and are presented as means ± SEM. One-way or two-way ANOVA was performed where appropriate, and differences were considered statistically significant at $P < 0.05$.

RESULTS

We first validated the model used here to study the mechanisms by which adiponectin improved insulin sensitivity. Temporal analysis after 2, 4, and 6 weeks of HFD of the area under curve on the GTT (Fig. 1*A*), plasma insulin (Fig. 1*B*), plasma glucose (Fig. 1*C*), and HOMA-insulin resistance (Fig. 1*D*) indicated an exaggerated and more rapid development of insulin insensitivity in Ad-KO mice fed the HFD compared with wild-type (WT) mice. This was reflected in significantly reduced insulin-stimulated phosphorylation of IRS (Y612) and Akt (S473) in the skeletal muscle of Ad-KO mice at 4 and 6 weeks, yet only after 6 weeks in WT mice (Fig. 1*E* and *F*). Original Western blot data are shown for all insulin-signaling analyses in Supplementary Fig. 1. A detailed investigation of insulin sensitivity using the hyperinsulinemic-euglycemic clamp in these mice demonstrated impaired glucose homeostasis in Ad-KO mice after only 2 weeks of the HFD. This was evident from the decreased glucose infusion rate (Fig. 2*A*) and insulin-altered glucose appearance rate (Fig. 2*B* and *E*), despite an increased glucose disappearance rate (Fig. 2*C* and *E*). After 2 weeks of the HFD, but not after 6 weeks (17), we observed an elevation in insulin-stimulated glucose uptake in skeletal muscle, indicating an important initial compensatory role of skeletal muscle in maintaining whole-body glucose homeostasis in the Ad-KO mouse. No difference was observed in the glycolytic rate in Ad-KO mice fed chow or the HFD for 2 weeks (Fig. 2*D*).

We next examined changes in oxidative stress and observed a rapid, significant decrease in SOD activity after 2 weeks of the HFD in Ad-KO but not WT mice (Fig. 3*A*). After 4 weeks, the HFD induced a decrease in SOD activity in both groups of mice. Interestingly, this decreased SOD activity was transient and recovered in both WT and HFD mice after 6 weeks of the HFD (Fig. 3*A*). Under chow-fed conditions, Ad-KO mice had a lower GSH-to-GSSG ratio than WT mice (Fig. 3*B*), and the GSH-to-GSSG ratio increased in the muscle of Ad-KO mice after 4 and 6 weeks of the HFD (Fig. 3*B*). The WT mice showed an apparent decrease after 2 weeks and a significant decrease in the GSH-to-GSSG ratio after 4 weeks of the HFD (Fig. 3*B*).

After replenishing normal circulating levels of adiponectin to the Ad-KO mice, we observed that the HFD-induced decrease in SOD activity was corrected (Fig. 3*C*). Furthermore, analysis of lipid peroxidation using the TBARS assay confirmed an elevated level of oxidative stress in muscle of Ad-KO mice after 2 weeks of the HFD, and this was corrected in mice that received adiponectin replenishment (Fig. 3*D*). Analysis of ROS generation in response to palmitate in vitro using L6 myotubes confirmed the effect of adiponectin on preventing free fatty acid–induced oxidative stress (Fig. 3*E*). We measured glucose uptake in primary skeletal muscle cells to determine changes in insulin sensitivity and found that adiponectin enhanced sensitivity of cells to a submaximal (10 nmol/L) insulin concentration and that palmitate-induced insulin resistance was alleviated in the presence of adiponectin (Fig. 3*F*).

To further investigate potential mechanisms underlying these changes, we performed gene array analysis of

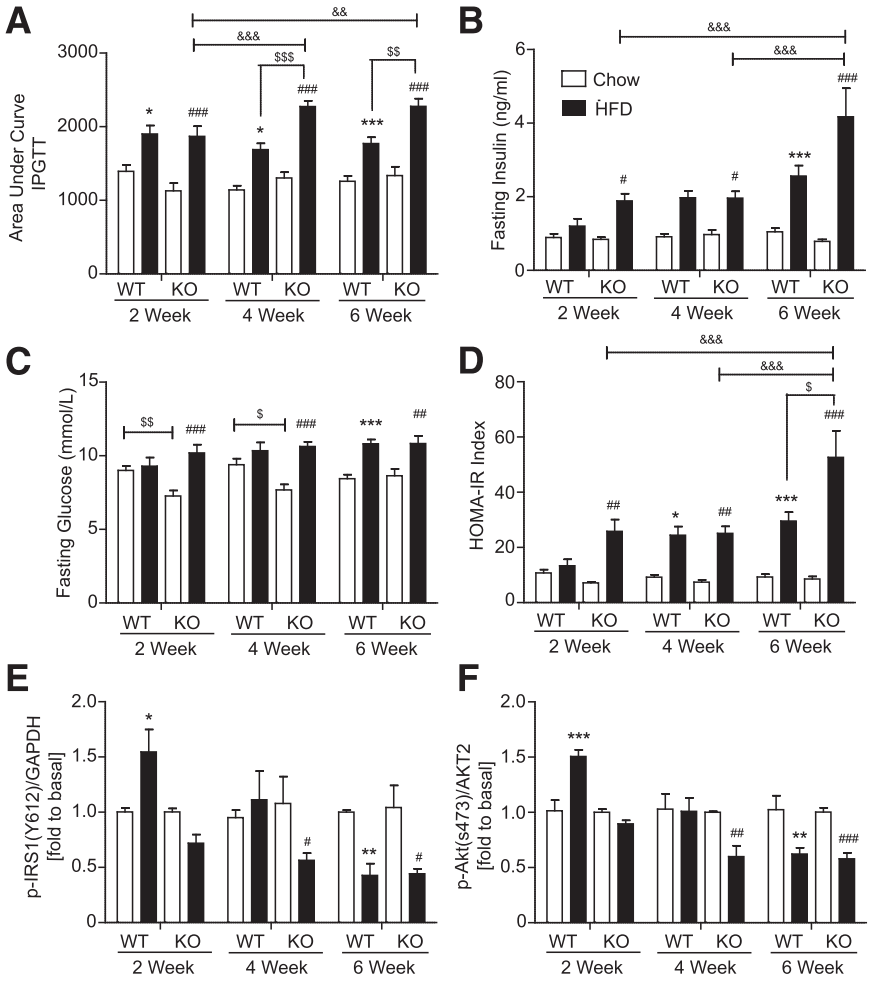

Figure 1—Metabolic characterization of WT and Ad-KO mice with and without adiponectin administration. The WT or Ad-KO mice were fed regular chow (Chow) or a 60% HFD at the age of 6 weeks for 2, 4, or 6 weeks. Mice were weighed and experiments performed, or serum samples collected for analysis after 5–6 h fasting. Skeletal muscle insulin signaling was assessed 15 min after a bolus injection of insulin (4 units/kg body weight) in the tail vein. During intraperitoneal GTT (IPGTT), blood samples were collected and the glucose level was determined 15, 30, 60, and 90 min after a bolus intraperitoneal injection of glucose. *A*: IPGTT area under curve. *B*: Fasting insulin level before IPGTT (ng/mL). *C*: Fasting glucose level before IPGTT (mmol/L). *D*: HOMA for insulin resistant (IR) was calculated as [fasting glucose (mmol/L) × fasting insulin (mU/L)]/22.5. *E* and *F*: Quantitative analysis of Western blots to determine insulin-stimulated phosphorylated (p)-Akt (S473) and p-IRS1 (Y612) in skeletal muscle. The p-Akt data were corrected by total Akt2, and the pIRS1 data were corrected by GAPDH. Data represent mean ± SEM (n = 5–11). *Significant difference between HFD and Chow in WT mice. #Significant difference between HFD and Chow in Ad-KO. $Significant difference between WT and Ad-KO mice. &Significant difference during time course within one genotype. *,#,$,&$P < 0.05$; **,##,$$,&&$P < 0.01$; ***,###,$$$,&&&$P < 0.001$.

those implicated in regulation of oxidative stress. Within a total of 84 genes that were analyzed, the HFD altered the expression of genes involved in the regulation not only of GSH peroxidase, peroxiredoxin, SOD, and superoxide metabolism but also oxidative stress–responsive and oxygen transporter genes (Fig. 4*A*). Adiponectin supplementation effectively reversed HFD-induced changes in the expression of several of the main antioxidant genes: Gpx1 and 3, SOD1 and 2, Prdx1, 3, and 4, and Ptgs 1 and 2 (Fig. 4*B*). The HFD also induced the ROS production gene Nox4, and a direct upregulation of the copper chaperone for SOD (Ccs) by adiponectin was also observed (Fig. 4*B*). A heat map with specific information on the full range of genes tested and changes therein are shown in Supplementary Fig. 2.

We used well-established markers to investigate temporal changes in skeletal muscle autophagy in these mice. HFD feeding for 6 weeks significantly increased levels of LC3-II in WT skeletal muscle, but this was not observed in Ad-KO mice (Fig. 5*A*). Original Western blot data are shown for all autophagy analysis in Supplementary Figs. 3 and 4. We found that replenishing adiponectin to Ad-KO mice restored the higher level of LC3-II expression (Fig. 5*B*). A decrease in p62 levels was observed at all time points in WT mouse muscle; however, accumulation of p62 was evident in Ad-KO mouse muscle (Fig. 5*C*), the latter being reduced by adiponectin supplementation (Fig. 5*D*). The enhanced LC3-II levels observed after 6 weeks of the HFD in WT mice correlated with enhanced expression of Beclin1 (Fig. 5*E*). Beclin1 expression did

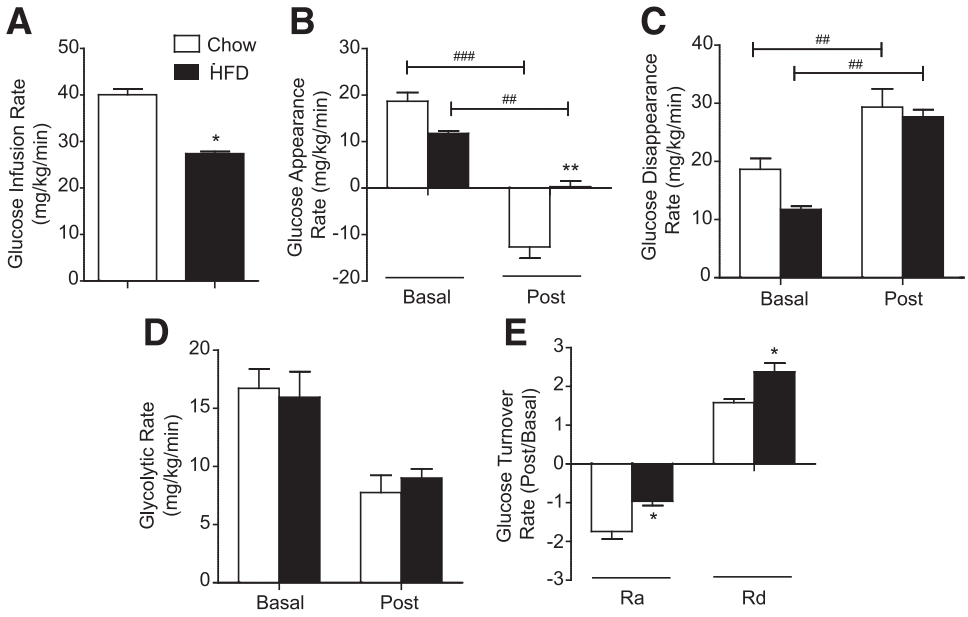

Figure 2—Hyperinsulinemic-euglycemic clamp analysis. Ad-KO mice were fed regular chow (Chow) or a 60% HFD at the age of 6 weeks for 2 weeks. Jugular vein and carotid artery catheters were embedded into animals 4 days before the hyperinsulinemic- euglycemic clamp procedure, and clamps were performed on animals after 5–6 h starvation. Blood samples were collected during the clamp procedure, and calculations were made based on the radioactivity readings from serum to represent whole-body glucose metabolism. *A*: Glucose infusion rate (mg/kg/min). *B*: Glucose appearance rate (Ra; mg/kg/min); *C*: Glucose disappearance rate (Rd; mg/kg/min). *D*: Glycolytic rate (mg/kg/min); *E*: Glucose turnover rate (fold change calculated by post [after insulin clamp]/basal [before insulin clamp]). Data represent mean ± SEM (n = 4–5). *Significant compared between HFD and Chow mice. #Significant difference between before (basal) and after (post) insulin clamp. *$P < 0.05$; **,##$P < 0.01$; ###$P < 0.001$.

not change in Ad-KO mice; however, adiponectin did induce Beclin1 expression in the muscle of these mice (Fig. 5*F*). Skeletal muscle FGF-21 content was enhanced after 2, 4, and 6 weeks of the HFD only in WT mice (Fig. 5*G*); however, replenishing adiponectin in Ad-KO mice led to increased FGF-21 expression (Fig. 5*H*). We also analyzed changes in expression of genes that play a key role at various stages of autophagic flux. Our data indicated that the HFD decreased the expression of several autophagy-related genes and that three of these, Beclin1, LC3, and ULK1, were corrected by adiponectin treatment (Fig. 5*I*).

We then examined changes in autophagy in cultured skeletal muscle cells treated with or without adiponectin. Conversion of LC3-I to LC3-II is the most widely used marker for autophagosomes, and when this was assessed by Western blotting (Fig. 6*A*), we found increased LC3-II levels after adiponectin treatment. We hypothesized that the mechanism by which adiponectin stimulated autophagy was by AMPK, and after inhibition of AMPK using compound C, adiponectin-stimulated LC3-II formation and phosphorylation of ULK1 on Ser555 was attenuated (Fig. 6*A*). Autophagosome formation in response to adiponectin was also confirmed by the punctate appearance of endogenous LC3 upon immunofluorescent detection (Fig. 6*B*). To more accurately examine autophagic flux, we generated skeletal muscle cells stably overexpressing RFP/GFP-LC3. This approach is advantageous in that it allows analysis of autophagic flux because GFP, but not RFP, is sensitive to quenching by the acidic environment of the autophagolysosome. We observed that adiponectin initially stimulated the punctate appearance of fluorescent LC3, whereas a comparison of merged images showing maintained red and decreased green fluorescence indicated completion of autophagic flux in response to adiponectin (Fig. 6*C*).

Lysosomal enzyme activity, measured using Magic Red, was increased in response to adiponectin (Fig. 6*D*). We used bafilomycin or chloroquine to inhibit autophagic flux and demonstrated that this led to decreased insulin-stimulated glucose uptake (Fig. 7*A*). Similarly, insulin-stimulated phosphorylation of IRS1 (Tyr612), Akt (Thr308), and Akt (Ser473) was attenuated under these conditions, as seen in the representative Western blots (Fig. 7*B*) and quantitative analysis (Fig. 7*C–E*). We also generated L6 skeletal muscle cells stably overexpressing the dominant-negative inhibitor of autophagy (Atg5K130R). In these autophagy-deficient cells, we also observed a reduction in insulin-stimulated phosphorylation of IRS1 and Akt, as seen in the representative Western blots (Fig. 7*F*) and quantitative analysis (Fig. 7*G–I*).

DISCUSSION

Numerous studies have demonstrated that adiponectin improves insulin sensitivity and alleviates metabolic dysfunction in skeletal muscle (2,19). Various mechanisms

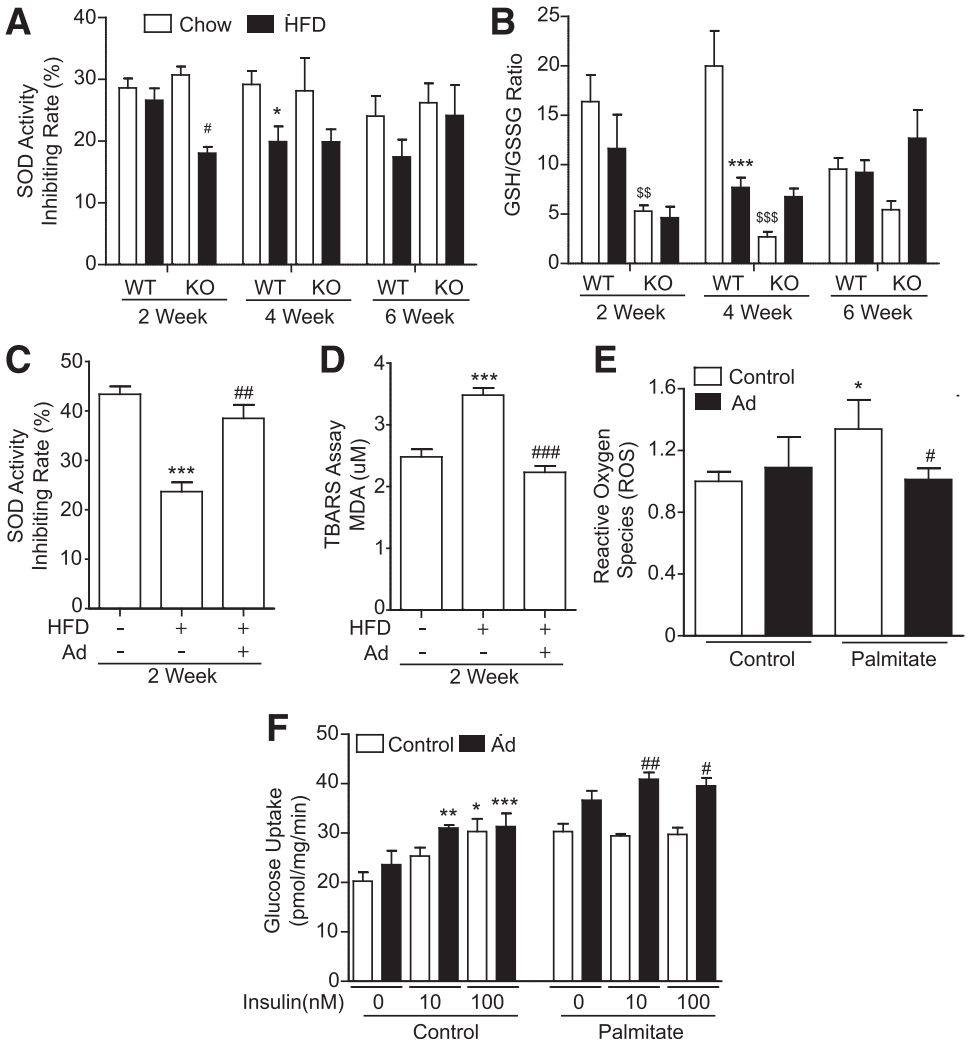

Figure 3—Analysis of oxidative stress in skeletal muscle. WT or Ad-KO mice were fed regular chow (Chow) or a 60% HFD at the age of 6 weeks for 2, 4, and 6 weeks. Skeletal muscle samples were collected after 5–6 h fasting for subsequent analysis of SOD activity (*A*) and the ratio between GSH over GSSG (*B*). Data represent mean ± SEM (n = 4–8). *Significant difference between HFD and Chow in WT mice. #Significant difference between HFD and Chow in KO mice. $Significant difference between WT and KO mice. *,#$P < 0.05$; $$$P < 0.01$; ***,$$$$P < 0.001$. KO mice were fed Chow or 60% HFD at the age of 6 weeks. After 2 weeks, mice were treated with saline (Chow, 60% HFD) or adiponectin (60% HF + Ad) at the dosage of 3 μg/g body weight twice daily by intraperitoneal injection for an additional week. Skeletal muscle samples were collected after 5–6 h starvation to analyze SOD activity (*C*) and for TBARS assay (*D*). MDA, malondialdehyde. Data represent mean ± SEM (n = 6–7). *Significant difference comparing HFD and Chow; #Significant difference between saline- and adiponectin-treated HFD-fed mice. ##$P < 0.01$; ***,###$P < 0.001$. Primary skeletal muscle cells isolated from C57BL6 mice were cultured with or without adiponectin (5 μg/mL) until differentiated into myotubes and then treated with 250 μmol/L palmitate for 2 h (*E*) and 48 h (*F*), followed by analysis of oxidative stress by ROS production (*E*) and insulin resistance by glucose uptake (*F*). *E*: Flow cytometry was used to detect intracellular ROS, followed by H2DCFDA (2',7'-dichlorodihydrofluorescein diacetate) staining for 30 min. *F*: Insulin was used at submaximal (10 nmol/L) and maximal (100 nmol/L) concentrations during the final 1 h before the glucose uptake assay (pmol/mg/min). Data represent mean ± SEM (n = 4–5). *Significant difference compared with control. #Significant difference compared with palmitate treatment. *,#$P < 0.05$; **,##$P < 0.01$; ***$P < 0.001$.

by which adiponectin acts have been established; yet, further detailed investigation and uncovering of novel aspects is needed. Here, we used WT and Ad-KO (with and without adiponectin replenishment) mice fed chow or HFD. We previously validated that HFD-fed Ad-KO mice developed skeletal muscle insulin resistance and glucose intolerance and that replenishment of adiponectin corrected these defects (17). We also conducted a metabolomic profiling analysis and found that adiponectin alleviated HFD-induced changes in metabolites such as several diacylglycerol species, branched-chain amino acids, and various lysolipids (17). Here, an important goal of our study was to analyze temporal changes (at 2, 4, and 6 weeks) in glucose homeostasis (GTT and hyperinsulinemic-euglycemic clamp) and skeletal muscle insulin sensitivity to confirm an exaggerated and more rapid effect in Ad-KO mice, which was alleviated by administering recombinant adiponectin.

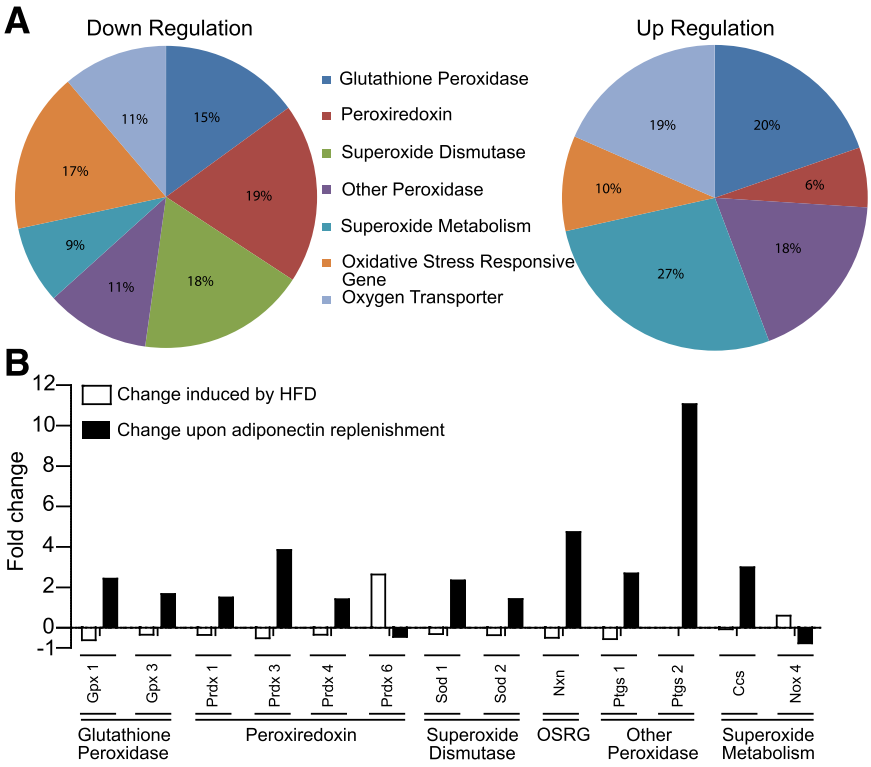

Figure 4—Oxidative stress gene array. Ad-KO mice were fed regular chow or a 60% HFD at the age of 6 weeks. After 2 weeks, the mice were treated with saline or adiponectin at a dosage of 3 μg/g body weight twice daily by intraperitoneal injection for an additional week. Skeletal muscle samples were collected after 5–6 h starvation, and mRNA was extracted and analyzed by PCR array. *A*: Pie chart of the global data set (84 genes) indicating differentially expressed genes after HFD treatment categorized by pathways involved in the regulation of oxidative stress. *B*: Quantitative analysis of gene expressions that were most highly altered by HFD and/or adiponectin administration (n = 4–5).

Oxidative stress is well established as a causative factor in the development of skeletal muscle insulin resistance and mitochondrial dysfunction and one that can be modified by adiponectin (3,4,18,20). One conclusion from our current study is that the ability of adiponectin to correct HFD-induced reductions in antioxidant gene expression is one of the mechanisms by which adiponectin exerts its insulin-sensitizing effect in skeletal muscle and improves peripheral glucose homeostasis. SOD, catalase, and GSH peroxidase are major antioxidative enzymes with which cells are equipped to fight damage caused by ROS (21,22). The increased expression of these antioxidative enzymes was indeed correlated with measures of oxidative stress, such as the GSH-to-GSSG ratio and SOD activity, and the TBARS assay to assess lipid peroxidation. One additional interesting observation we made was that Ad-KO mice had higher initial oxidative stress level than the WT mice. The elimination of ROS can also be catalyzed by nitric oxide synthase (Nos2), and we observed that expression of this enzyme was reduced by the HFD and induced by adiponectin. Other studies have demonstrated that adiponectin reduced oxidative stress by downregulating NADPH oxidase by inactivating the phosphorylation of $p47^{phox}$, the regulatory subunit of NADPH oxidase (23). Many studies have now established an important crosstalk between oxidative stress and autophagy (24), although the significance in terms in skeletal muscle metabolism (9–12,14,15) requires further investigation.

An important and novel focus of our study, therefore, was the analysis of skeletal muscle autophagy (9–12,14,15). First, increased LC3-II and decreased p62 levels indicated that HFD induced autophagy in skeletal muscle (25). The increased induction of autophagy may be at least partly due to an increase in Beclin1, which has a well-characterized role in the induction of autophagosome formation (25). No studies to date have documented the regulation of skeletal muscle autophagy by adiponectin; however, in recent months, direct regulation of autophagy by adiponectin has been shown in liver and macrophages (26,27). Importantly, we found that the induction of skeletal muscle autophagy observed in WT mice was not apparent in Ad-KO mice. However, replenishing adiponectin to the circulation of HFD-fed Ad-KO mice restored the increase in LC3-II formation and reduced accumulation of p62. On the basis of our data and recent studies that have begun to document the association between skeletal muscle autophagy and metabolism (9,10,28,29), we propose an important role of adiponectin in the ability of skeletal muscle to elevate autophagy in response to an HFD.

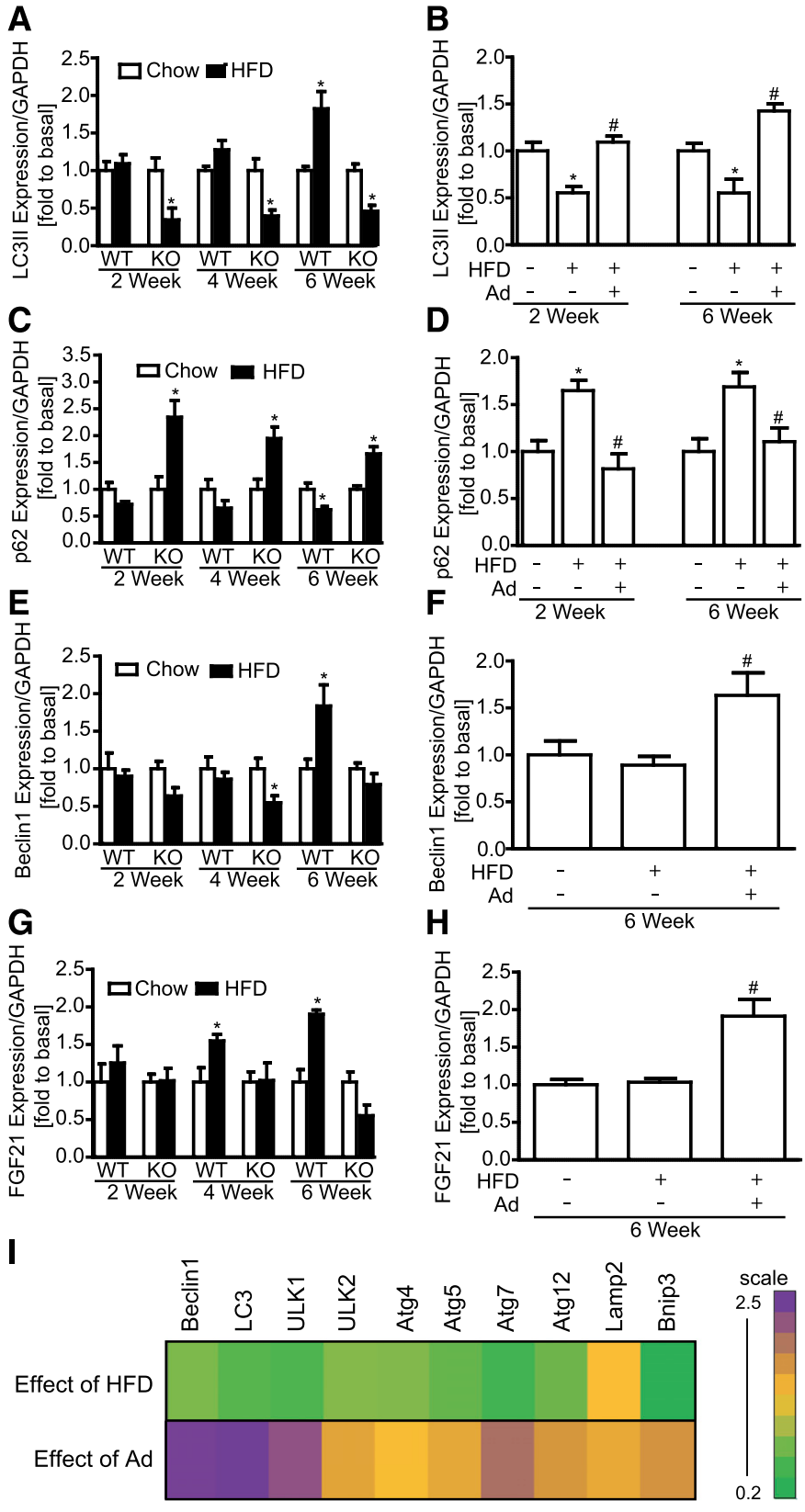

Figure 5—Analysis of skeletal muscle autophagy using Western blotting. WT or Ad-KO mice were fed regular chow (Chow) or a 60% HFD at the age of 6 weeks for of 2, 4, and 6 weeks. In additional studies with Ad-KO mice, after 2 weeks and 6 weeks, these mice were treated with saline or adiponectin at a dosage of 3 μg/g body weight twice daily by intraperitoneal injection for 1 additional week and 2 weeks, respectively. Skeletal muscle samples were collected after 5–6 h fasting for subsequent analysis by Western blotting. In WT and KO animals fed Chow or the HFD for 2, 4, and 6 weeks, we examined expression of LC3II (*A*), p62 (*C*), Beclin1 (*E*), and FGF21 (*G*), all corrected for GAPDH content (n = 8). We also examined the effect of adiponectin replenishment after 2 or 6 weeks of the HFD in Ad-KO mice on

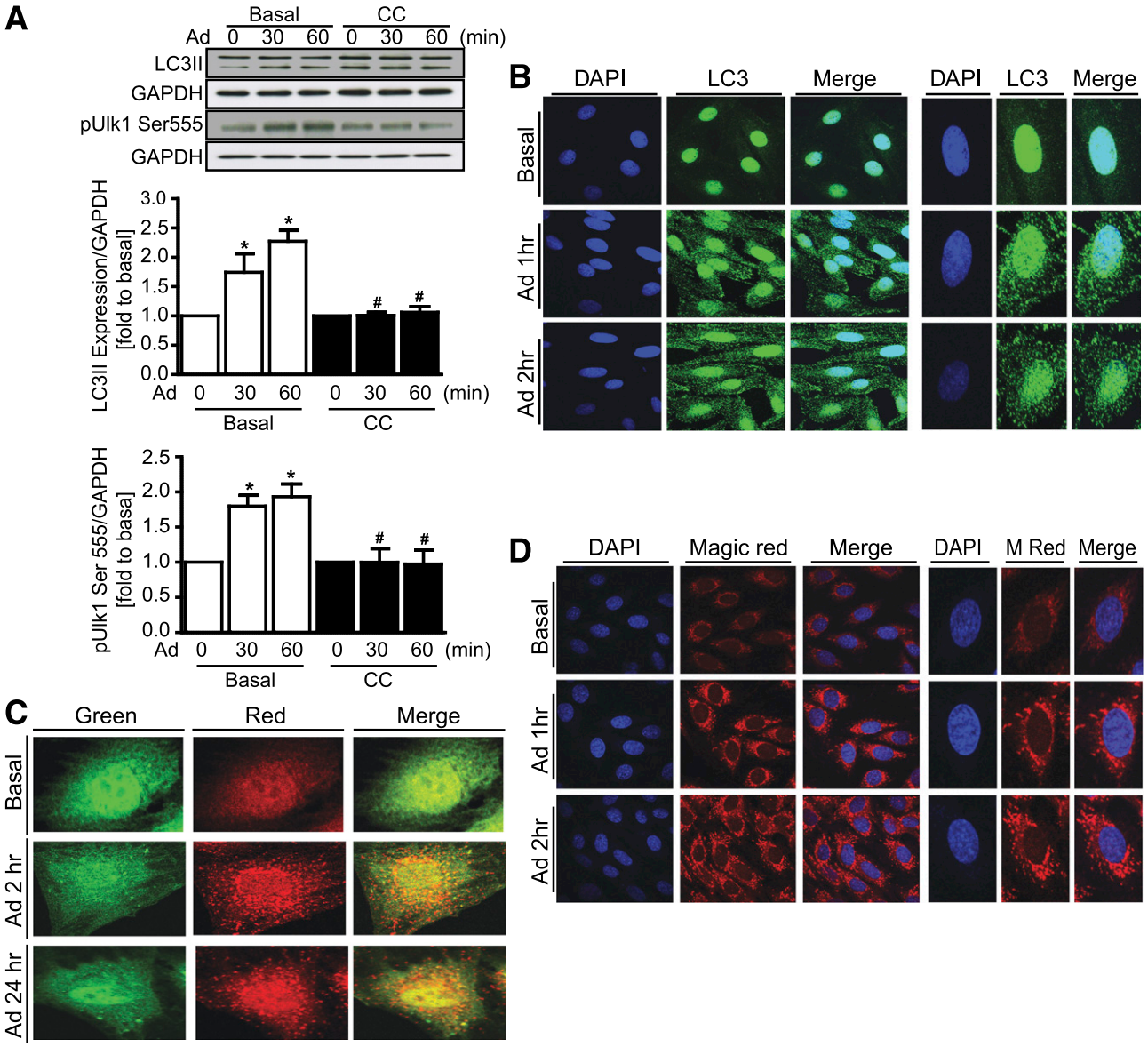

Figure 6—Stimulation of autophagy flux by adiponectin in L6 cells. *A*: L6 cells were treated with adiponectin (5 μg/mL) for 30 or 60 min in the presence or absence of compound C (CC; 10 μmol/L, 1 h), then LC3II and phospho-Ulk1 (Ser555), analyzed by Western blotting cell lysates. Representative images and quantitation of three to five experiments (mean ± SEM) are shown. *$P < 0.05$ comparing control vs. adiponectin treatment; #$P < 0.05$ compared with respective adiponectin time without compound C. *B*: Immunofluorescent detection of intracellular endogenous LC3II by confocal microscopy. Nucleus was identified using DAPI. Representative images for DAPI, LC3II, and the merged image are shown on the left side, with higher magnification of single cells on the right side. *C*: Analysis of tandem RFP/GFP-LC3 expressing L6 cells showing representative images from three of the relative GFP and RFP signals, and the merged image. *D*: Representative fluorescence images of Magic Red (M Red) and cathepsin B activity were detected by confocal microscopy.

To further investigate this observation, we then examined whether adiponectin directly induced autophagy in skeletal muscle cells. We measured autophagic flux using a combination of approaches to determine autophagosome formation and autophagolysosomal formation and activity (25), all of which demonstrated that adiponectin directly stimulated autophagic flux. Our data on stimulation of autophagy by adiponectin adds a novel perspective

expression of LC3II (*B*), p62 (*D*), Beclin1 (*F*), and FGF21 (*H*) ($n = 8$). *$P < 0.05$ compared with Chow; #$P < 0.05$ comparing HFD + Ad with HFD alone. *I*: Expression of autophagy-related genes was also determined by RT-PCR ($n = 6$), and changes in relative expression levels are shown as fold changes in a heat map.

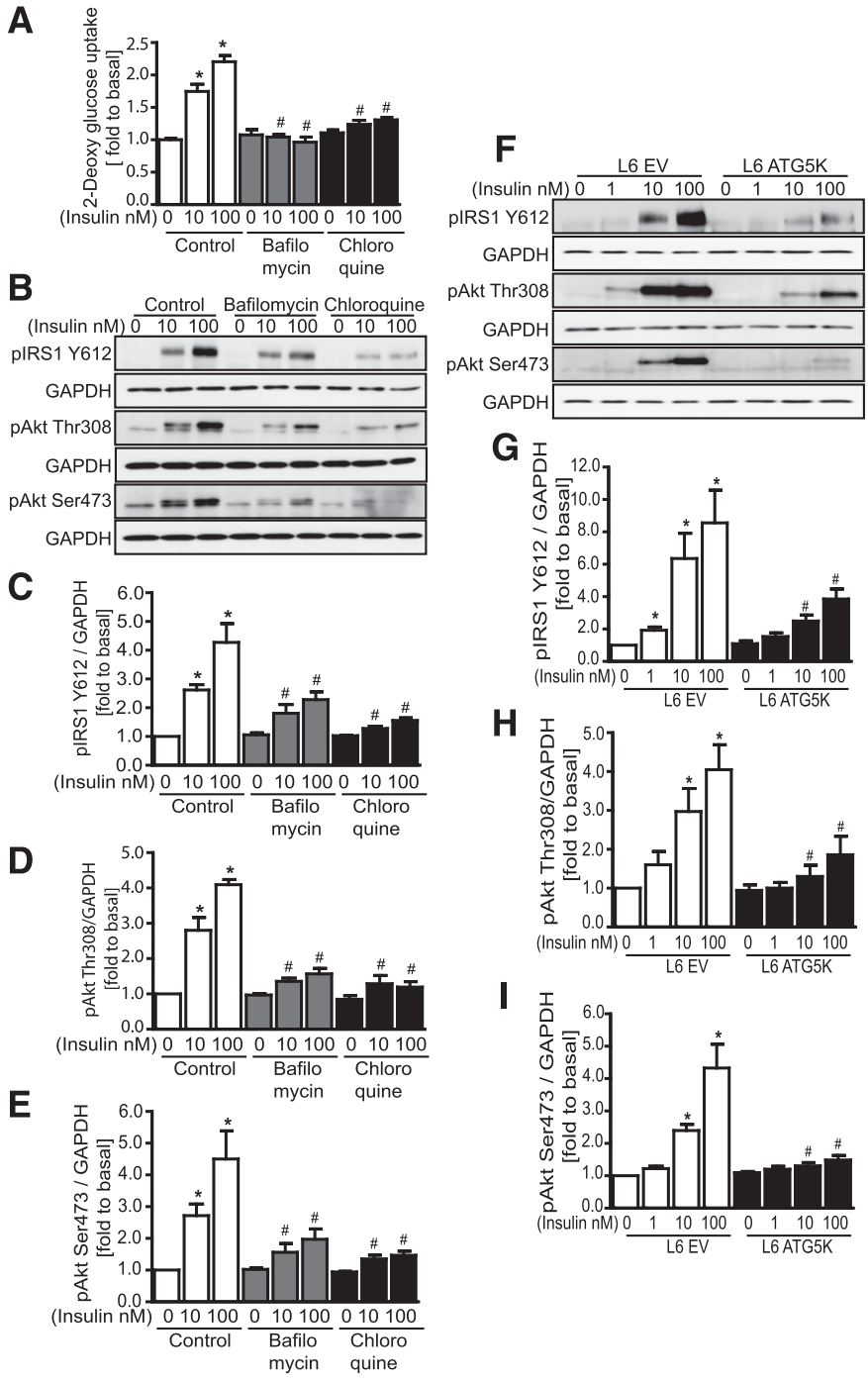

Figure 7—Functional significance of altered autophagy on insulin sensitivity. *A*: L6 cells stably overexpressing GLUT4-myc were pretreated with or without bafilomycin (200 nmol/L, 24 h) or chloroquine (100 μmol/L, 24 h) and stimulated with insulin (10 or 100 nmol/L, 20 min) before analysis of glucose uptake. *B–E*: Cells were pretreated with or without bafilomycin or chloroquine and stimulated with insulin (10 or 100 nmol/L, 5 min), then cell lysates were prepared to determine phosphorylation of IRS Y612 (*B* and *C*), Akt T308 (*B* and *D*), and Akt S473 (*B* and *E*). An autophagy-deficient stable cell line was created using Atg5K130R overexpression, and comparing these cells (Atg5K) vs. cells infected with empty vector (EV) shows that insulin sensitivity (1, 10, and 100 nmol/L, 5 min) was attenuated (*F–I*) (n = 3–5). *$P < 0.05$ compared with no insulin. #$P < 0.05$ comparing insulin action in the Atg5K cells vs. EV cells.

to the growing body of work documenting the relationship of skeletal muscle autophagy with insulin sensitivity and metabolism. For example, exercise stimulated skeletal muscle autophagy, and autophagy-deficient mice also exhibited altered glucose metabolism during acute exercise as well as impaired chronic exercise–mediated protection against HFD-induced glucose intolerance (10). Others have reported activation of autophagy in skeletal muscle in response to exercise and caloric restriction (11–14). Furthermore, starvation-induced autophagic

flux was greater in glycolytic versus highly oxidative muscle, and this was related to AMPK and mammalian target of rapamycin activities, which are both important determinants of autophagy (11,13,30,31). The regulatory events required to induce autophagy were attenuated with aging in skeletal muscle (15). We investigated the mechanistic role of AMPK in mediating the stimulation of autophagic flux in skeletal muscle cells in response to adiponectin and observed that the well-established target of AMPK in inducing autophagy, ULK1 phosphorylation on Ser555, was directly increased by adiponectin. Furthermore, stimulation of LC3-II levels and phospho-ULK1 by adiponectin were attenuated upon inhibition of AMPK, confirming an important role of AMPK signaling (26,32). Thus, our current data and recent literature both suggest that induction of skeletal muscle autophagy by various stimuli gives rise to beneficial metabolic effects.

Perhaps the most striking observation in recent literature was that autophagy-deficient mice with skeletal muscle–specific deletion of Atg7 were protected from diet-induced obesity and insulin resistance (9). Mechanistically, mitochondrial dysfunction in this model was overcome by autophagy-dependent FGF-21 expression in skeletal muscle after 13 weeks of the HFD. This FGF-21 acted as a myokine to mediate peripheral effects leading to protection from diet-induced obesity and insulin resistance (9). We investigated FGF-21 expression in skeletal muscle of HFD-fed WT and Ad-KO mice, and our data indicated that only skeletal muscle from WT, but not Ad-KO mice, had elevated FGF-21 content. This suggests that HFD-induced autophagy and FGF-21 production were dependent on adiponectin, and we also observed that adiponectin directly induced FGF-21 expression in cultured skeletal muscle cells. Interestingly, there are two recently published reports that the beneficial metabolic effects of FGF-21 are mediated via adiponectin action (33,34). Thus, conceivably, adiponectin may act as a front- and back-end master regulator of FGF-21 physiology. The reciprocal interactions between autophagy and oxidative stress (11) should also be further investigated, for example, using autophagy-deficient animal models.

In summary, this work significantly extends our understanding of mechanisms by which adiponectin alleviates HFD-induced insulin resistance and metabolic dysfunction in skeletal muscle. In particular, we document that HFD-induced obesity elicits increased skeletal muscle autophagy and for the first time show the facilitatory role of adiponectin in this process. We propose that adiponectin stimulates autophagic flux in skeletal muscle, especially under pathological conditions, and that this represents an important mechanistic component of its beneficial metabolic effects. Nevertheless, other cellular events, such as oxidative stress, precede changes in autophagy, and autophagy itself may still be viewed as a doubled-edged sword whereby too much or too little and the temporal nature of the process can determine distinct cellular consequences (7,8).

Funding. This work was supported by an operating grant to G.S. from Canadian Institutes of Health Research. G.S. also acknowledges Career Investigator support from the Heart & Stroke Foundation of Ontario.

Duality of Interest. No potential conflicts of interest relevant to this article were reported.

Author Contributions. Y.L. performed most of the experimental work, researched the work, and helped plan protocols and experiments and with writing the manuscript. R.P., E.R., M.P., and T.V.G. conducted the experimental work included in the figures. M.P.S. contributed to the design of the experimental work. A.X. contributed to planning the study, analyzing data, and editing the manuscript. G.S. designed the project, supervised the experimental work, wrote the manuscript, and provided funding. G.S. is guarantor of this work and, as such, had full access to all the data in the study and takes responsibility for the integrity of the data and the accuracy of the data analysis.

References

1. Liu Y, Retnakaran R, Hanley A, Tungtrongchitr R, Shaw C, Sweeney G. Total and high molecular weight but not trimeric or hexameric forms of adiponectin correlate with markers of the metabolic syndrome and liver injury in Thai subjects. J Clin Endocrinol Metab 2007;92:4313–4318

2. Turer AT, Scherer PE. Adiponectin: mechanistic insights and clinical implications. Diabetologia 2012;55:2319–2326

3. Newsholme P, Gaudel C, Krause M. Mitochondria and diabetes. An intriguing pathogenetic role. Adv Exp Med Biol 2012;942:235–247

4. Samuel VT, Shulman GI. Mechanisms for insulin resistance: common threads and missing links. Cell 2012;148:852–871

5. Combs TP, Pajvani UB, Berg AH, et al. A transgenic mouse with a deletion in the collagenous domain of adiponectin displays elevated circulating adiponectin and improved insulin sensitivity. Endocrinology 2004;145:367–383

6. Ge Q, Ryken L, Noel L, Maury E, Brichard SM. Adipokines identified as new downstream targets for adiponectin: lessons from adiponectin-overexpressing or -deficient mice. Am J Physiol Endocrinol Metab 2011;301:E326–E335

7. Gurusamy N, Das DK. Is autophagy a double-edged sword for the heart? Acta Physiol Hung 2009;96:267–276

8. Kubisch J, Türei D, Földvári-Nagy L, et al. Complex regulation of autophagy in cancer-integrated approaches to discover the networks that hold a double-edged sword. Semin Cancer Biol 2013;23:252–261

9. Kim KH, Jeong YT, Oh H, et al. Autophagy deficiency leads to protection from obesity and insulin resistance by inducing Fgf21 as a mitokine. Nat Med 2013;19:83–92

10. He C, Bassik MC, Moresi V, et al. Exercise-induced BCL2-regulated autophagy is required for muscle glucose homeostasis. Nature 2012;481:511–515

11. Mofarrahi M, Guo Y, Haspel JA, et al. Autophagic flux and oxidative capacity of skeletal muscles during acute starvation. Autophagy 2013;9:1604–1620

12. Lira VA, Okutsu M, Zhang M, et al. Autophagy is required for exercise training-induced skeletal muscle adaptation and improvement of physical performance. FASEB J 2013;27:4184–4193

13. Cui M, Yu H, Wang J, Gao J, Li J. Chronic caloric restriction and exercise improve metabolic conditions of dietary-induced obese mice in autophagy correlated manner without involving AMPK. Diabetes Res 2013;2013:852754

14. Jamart C, Naslain D, Gilson H, Francaux M. Higher activation of autophagy in skeletal muscle of mice during endurance exercise in the fasted state. Am J Physiol Endocrinol Metab 2013;305:E964–E974

15. Kim YA, Kim YS, Oh SL, Kim HJ, Song W. Autophagic response to exercise training in skeletal muscle with age. J Physiol Biochem 2013;69:697–705

16. Wang Y, Li YB, Yin JJ, et al. Autophagy regulates inflammation following oxidative injury in diabetes. Autophagy 2013;9:272–277

17. Liu Y, Turdi S, Park T, et al. Adiponectin corrects high-fat diet-induced disturbances in muscle metabolomic profile and whole-body glucose homeostasis. Diabetes 2013;62:743–752
18. Ceddia RB, Somwar R, Maida A, Fang X, Bikopoulos G, Sweeney G. Globular adiponectin increases GLUT4 translocation and glucose uptake but reduces glycogen synthesis in rat skeletal muscle cells. Diabetologia 2005;48:132–139
19. Liu Y, Sweeney G. Adiponectin action in skeletal muscle. Best Pract Res Clin Endocrinol Metab 2014;28:33–41
20. Matsuda M, Shimomura I. Roles of adiponectin and oxidative stress in obesity-associated metabolic and cardiovascular diseases. Rev Endocr Metab Disord 2014;15:1–10
21. Roberts CK, Barnard RJ, Sindhu RK, Jurczak M, Ehdaie A, Vaziri ND. Oxidative stress and dysregulation of NAD(P)H oxidase and antioxidant enzymes in diet-induced metabolic syndrome. Metabolism 2006;55:928–934
22. Förstermann U. Nitric oxide and oxidative stress in vascular disease. Pflugers Arch 2010;459:923–939
23. Carnevale R, Pignatelli P, Di Santo S, et al. Atorvastatin inhibits oxidative stress via adiponectin-mediated NADPH oxidase down-regulation in hypercholesterolemic patients. Atherosclerosis 2010;213:225–234
24. Yuzefovych LV, LeDoux SP, Wilson GL, Rachek LI. Mitochondrial DNA damage via augmented oxidative stress regulates endoplasmic reticulum stress and autophagy: crosstalk, links and signaling. PLoS ONE 2013;8:e83349
25. Klionsky DJ, Abdalla FC, Abeliovich H, et al. Guidelines for the use and interpretation of assays for monitoring autophagy. Autophagy 2012;8:445–544
26. Lin Z, Wu F, Lin S, et al. Adiponectin protects against acetaminophen-induced mitochondrial dysfunction and acute liver injury by promoting autophagy in mice. J Hepatol 2014 May 29 [Epub ahead of print]
27. Qi GM, Jia LX, Li YL, Li HH, Du J. Adiponectin suppresses angiotensin II-induced inflammation and cardiac fibrosis through activation of macrophage autophagy. Endocrinology 2014;155:2254–2265
28. Wu JJ, Quijano C, Chen E, et al. Mitochondrial dysfunction and oxidative stress mediate the physiological impairment induced by the disruption of autophagy. Aging (Albany, NY Online) 2009;1:425–437
29. Wen H, Gris D, Lei Y, et al. Fatty acid-induced NLRP3-ASC inflammasome activation interferes with insulin signaling. Nat Immunol 2011;12:408–415
30. Castets P, Rüegg MA. MTORC1 determines autophagy through ULK1 regulation in skeletal muscle. Autophagy 2013;9:1435–1437
31. Castets P, Lin S, Rion N, et al. Sustained activation of mTORC1 in skeletal muscle inhibits constitutive and starvation-induced autophagy and causes a severe, late-onset myopathy. Cell Metab 2013;17:731–744
32. Nepal S, Park PH. Activation of autophagy by globular adiponectin attenuates ethanol-induced apoptosis in HepG2 cells: involvement of AMPK/FoxO3A axis. Biochim Biophys Acta 2013;1833:2111–2125
33. Lin Z, Tian H, Lam KS, et al. Adiponectin mediates the metabolic effects of FGF21 on glucose homeostasis and insulin sensitivity in mice. Cell Metab 2013;17:779–789
34. Holland WL, Adams AC, Brozinick JT, et al. An FGF21-adiponectin-ceramide axis controls energy expenditure and insulin action in mice. Cell Metab 2013;17:790–797